Journal of Alloys and Compounds 621 (2015) 283–286

Contents lists available at ScienceDirect

Journal of Alloys and Compounds

journal homepage: www.elsevier.com/locate/jalcom

Peritectic reaction on the Al-rich side of Al–Cr system

Güven Kurtuldu [a,*], Peter Jessner [b], Michel Rappaz [a]

[a] Computational Materials Laboratory, Institute of Materials, Ecole Polytechnique Fédérale de Lausanne, Station 12, CH-1015 Lausanne, Switzerland
[b] Constellium CRV, ZI Centralp, 0725 rue Aristide Bergés, BP 27, Voreppe FR-38341, France

ARTICLE INFO

Article history:
Received 22 August 2014
Accepted 23 September 2014
Available online 2 October 2014

Keywords:
Al–Cr
Phase diagram
Peritectic
Eutectic
Planar front solidification

ABSTRACT

A long lasting controversy on the nature of the reaction between liquid, Al and $Al_{45}Cr_7$ has been ended by planar front solidification experiments of Al–Cr alloy in a Bridgman furnace. Cr depletion in the liquid ahead of the quenched planar interface proves without any ambiguity that the invariant reaction on the Al-rich side of the Al–Cr phase diagram is peritectic. A value of the diffusion coefficient of Cr in liquid Al, $D_\ell = 2.4 \times 10^{-9}$ m^2/s, was also deduced from the solute composition profile measured in the quenched liquid.

1. Introduction

The binary Al–Cr system has been studied by many authors because of the existence of several structurally complex phases on the Al-rich side of the phase diagram [1–4]. For example, $Al_{45}Cr_7$ (or $Al_{13}Cr_2$, or Al_7Cr), $Al_{11}Cr_2$ (or Al_5Cr) and Al_4Cr are some of the known complex phases that exist in this region. The crystal structures of these intermetallic phases are similar and produce closely similar diffraction patterns [5–7]. They are described in terms of an arrangement of icosahedral clusters and have a close relation with the structure of an icosahedral quasicrystal Al_4Cr, which can form under rapid solidification conditions [1]. At lower Cr content, this phase reacts peritectically with the melt to form $Al_{11}Cr_2$, which in turn can react with the liquid to form $Al_{45}Cr_7$ by a peritectic reaction. The solid solubility of Cr in Al is limited, only 0.7 wt% at 661.5 °C, decreasing to 0.03 wt% at 350 °C [4].

On the nature of the invariant reaction between the liquid, the fcc-Al phase and $Al_{45}Cr_7$, there is a long-lasting controversy: the fcc-Al phase was considered to form with a peritectic reaction by Fink and Freche (1933) [8], Bradley et al. (1937) [9], Harding and Raynor (1952) [5], Zoller (1960) [10] and Murray (1998) [4], while Goto and Dogane (1927) [11], Neto et al. (1992) [12], Mahdouk and Gachon (2000) [3], Du et al. (2005) [13], Okamoto (2008) [14], Grushko et al. (2008) [2] and Almeida and Vilar (2010) [15] proposed a eutectic reaction.

Phase diagrams of Al binary alloys with transition metals demonstrate that Al–Ti and Al–V show a peritectic reaction, while Al–Mn, Al–Fe, Al–Co and Al–Ni exhibit a eutectic reaction on the Al-rich side [16]. Cr is at the point where the nature of the invariant reaction changes from peritectic to eutectic in the same row of the periodic table. The invariant reaction temperature is very close to the melting point of pure Al (660.452 °C) and the small temperature difference reported in the previous studies shows significant discrepancies. In most of these studies, the nature of the reaction was identified by thermal analysis of Al–Cr alloys and the invariant reaction temperature was determined during heating. However, trace impurities present in the alloys, contamination from the environment during their preparation and the accuracy of the temperature measurement bring uncertainties that do not allow an unambiguous identification of this reaction.

Two recent studies have been performed to just define the reaction type between fcc-Al, $Al_{45}Cr_7$ and the liquid. Du et al. [13] have carried out DSC experiments of Al–Cr samples at heating rates of 2, 5 and 10 K/min. They have prepared their samples by arc melting from 5N purity elements under carefully controlled Ar atmosphere. The alloys were subsequently annealed at 630 °C for 31 days under vacuum in quartz tubes and then quenched in water. Unfortunately, the authors did not perform a detailed compositional analysis on DSC samples after such a long annealing at such a high temperature and therefore the exact impurity levels in their alloys is not known. These authors demonstrated that the invariant reaction occurred 0.7 °C below the melting temperature of pure Al by extrapolating the onset temperature of fcc-Al melting for different heating rates, thus indicating a eutectic reaction.

Almeida and Vilar [15] have also proposed a eutectic reaction from microstructural observations of Al–Cr alloys prepared by laser alloying and subsequent laser melting. They have observed

* Corresponding author.

http://dx.doi.org/10.1016/j.jallcom.2014.09.174
0925-8388/

equiaxed cells containing fine $Al_{45}Cr_7$ particles dispersed in a fcc-Al phase separated by thin layers of fcc-Al. This morphology was explained as an indication of a solid–liquid interface where fcc-Al and $Al_{45}Cr_7$ are in contact with the liquid and grow simultaneously as is typically the case of a eutectic reaction.

As mentioned earlier, the difference between the invariant reaction temperature and the melting point of pure Al is very small so that the determination of the reaction type based on temperature measurements is very delicate. For example, iron is one of the main impurities in both Al and Cr, and the presence of Fe impurities in Al–Cr alloys decreases the onset temperature of the fcc-Al melting due to eutectic reaction between Al and Fe [17]. The determination of the onset temperature of fcc-Al melting on thermal curves upon heating can be significantly affected by the impurity levels [18,19]. On the other hand, the morphology of a solidified microstructure can be misleading and does not give a direct indication of the reaction type. For low and moderate solidification rates, a eutectic morphology generally solidifies as lamellae or fibers growing in a coupled mode perpendicular to the solidification front, whereas the peritectic alloy forms a primary phase surrounded by the peritectic phase (peritectic reaction and transformation). The microstructure therefore reflects the nature of the reaction, but this can be often insufficient and inconclusive. Peritectic phase can sometimes grow side by side with the primary phase giving the appearance of a coupled growth similar to coupled eutectics. This has been demonstrated over the past 20 years in Fe–Ni [20], Al–Ni [21] and Cu–Sn [22,23] at very low speed. In the case of Almeida and Vilar experiment [15], the microstructure might still look like a eutectic, since at high speed (20 mm/s) the microstructure becomes very fine with the primary phase being surrounded by peritectic one, as can be also seen in Al–Ti alloys [24].

2. Theory

In the present study, planar front growth solidification experiments were used to determine the type of invariant on the Al-rich side of the Al–Cr system. In such experiments, a binary alloy of nominal composition C_0 is solidified with a planar interface in a linear temperature gradient, G, and at constant pulling velocity v_p. Neglecting the nucleation stage, the first solid forms with a solute composition kC_0, where k is the partition coefficient defined as $k = C_s^*/C_\ell^*$ and C_s^* and C_ℓ^* are the equilibrium compositions of the solid and liquid, respectively. During growth, the solute balance at the interface leads to a depletion of solute elements in the liquid ahead of the interface if the slope of the liquidus is positive, which is the case of peritectic alloys, i.e., $k > 1$ (Fig. 1(a) and (b)), or on the opposite to a solute enrichment of the interfacial liquid if the slope of the liquidus is negative, which is the case of eutectic alloys, i.e., $k < 1$ (Fig. 1(c) and (d)). A diffusion boundary layer ahead of the solid–liquid interface builds up during an initial transient until steady state is reached. During this transient, the interfacial composition of the solid varies from kC_0 to C_0, while that of the liquid changes from C_0 to C_0/k . At steady state, the temperature of the solid–liquid is equal to that of the solidus and the actual velocity of the interface, v^*, is equal to the pulling velocity v_p. The steady-state solute profile in the liquid $C_\ell(z)$ is then given by:

$$C_\ell(z) = C_0\left\{1 + \frac{1-k}{k}\exp\left(-\frac{v_p z}{D_\ell}\right)\right\} \tag{1}$$

where z is the coordinate axis parallel to the solidification direction and attached to the moving solid–liquid interface, while D_ℓ is the diffusion coefficient of the solute element in the liquid. (Please note that this profile is slightly modified if one considers the liquid flow induced by solidification shrinkage). Associated with this

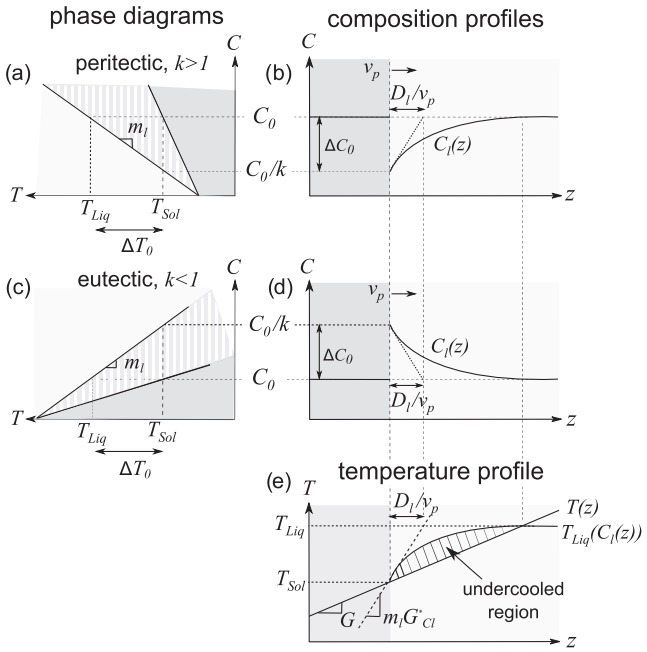

Fig. 1. Linear phase diagrams for (a) a peritectic alloy system, i.e., $k > 1$ and (c) a eutectic alloy system, i.e., $k < 1$. (b) and (d) show the corresponding composition profiles in the solid and liquid for a steady-state planar front solidification of a peritectic and eutectic alloy, respectively. If the liquidus temperature for the corresponding composition profile ahead of the solid–liquid interface is higher than the imposed temperature profile, an undercooled region forms as shown in (e).

steady-state solution is the formation of a constant solute boundary layer, the thickness of which is given by D_ℓ/v_p. The solute gradient ahead of the interface position, $G^*_{C\ell}$, is then given by

$$G^*_{C\ell} = \left(\frac{\partial C_\ell}{\partial z}\right)_{z=0} = -\frac{C_0(1-k)/k}{(D_\ell/v_p)} = -\frac{\Delta C_0}{(D_\ell/v_p)} \tag{2}$$

where $\Delta C_0 = C_0(1/k - 1)$ is the difference in composition between the liquid and solid phases at the interface, i.e., the difference of composition of the liquidus and solidus at the solidus temperature. If $k > 1$ (peritectic-type alloy), the gradient is positive, while if $k < 1$ (eutectic-type alloy), it is negative.

During directional solidification of an alloy in a Bridgman furnace, a planar solid–liquid interface can be maintained only if the solidification speed is small enough. The stability of a planar interface was discussed by Tiller et al. [25], in terms of the now well-known "constitutional supercooling" criterion which is illustrated in Fig. 1(e) for peritectic and eutectic alloys. If the actual temperature $T(z)$ imposed by the furnace ahead of the interface is higher than the local liquidus temperature $T_{Liq}(C_\ell(z))$, i.e., $T(z) \geqslant T_{Liq}(C_\ell(z))$, the planar interface will be stable. Because of the equality $T^* = T(z)|_{z=0} = T_{Liq}(C_\ell(z))|_{z=0} = T_{Liq}(C_\ell^*)$, the stability condition reduces to $\frac{\partial T(z)}{\partial z} \geqslant \frac{\partial T_{Liq}(C_\ell(z))}{\partial z}$. For a linearized phase diagram with a constant liquidus slope, m_ℓ, the stability condition for steady-state planar front solidification is given by:

$$G \geqslant m_\ell G^*_{C\ell} = \frac{\Delta T_0 v_p}{D_\ell} \tag{3}$$

where $\Delta T_0 = -m_\ell \Delta C_0$ is the equilibrium solidification interval of the alloy.

A critical velocity v_c for stable planar growth can be deduced by the limit of constitutional supercooling, i.e., $G = m_\ell G^*_{C\ell}$ or :

$$v_c = \frac{GD_\ell}{\Delta T_0} \tag{4}$$

3. Materials and methods

In this study, an Al–0.08 wt%Cr alloy with a low Cr content to avoid intermetallic formation was prepared in an induction furnace under Ar atmosphere from high purity Al (99.99 wt%) and Cr powder (99.5 wt%). It was then solidified in a Bridgman furnace under high thermal gradient, the details of which can be found in Ref. [22]. It just recalled that the hot stage is made of an induction coil which heats up a molybdenum susceptor, itself heating the specimen contained in a ceramic crucible, while the cold stage is a liquid metal bath. The effect of natural solutal convection in the specimen was limited by using small capillary alumina tubes with an inner diameter of 1.2 mm (outer diameter 2 mm, length 140 mm). Filling liquid metal into the capillary without any discontinuity was achieved by using an infiltration method. The alumina capillary was inserted inside an Al alloy cylinder (internal diameter 2 mm, out diameter 4 mm), which was previously drilled by wire electro-discharge machining. Two centering BN rings were attached to the capillary tube as shown in Fig. 2. The bottom of the capillary was closed with alumina paste. Another cylinder made of the same Al alloy was added on top of the capillary to provide enough material to fill the capillary at the center. The whole set-up was finally inserted in an alumina crucible (inner diameter 4 mm, outer diameter 7 mm and length 500 mm) and mounted in the Bridgman furnace.

After the sample was placed inside the furnace, the chamber and crucible were evacuated and purged with Ar gas three times. The susceptor was heated up to 900 °C at a controlled rate and the sample was maintained at this temperature for 15 min. The molten alloy, which had flown over the tip of the capillary, was then pushed inside the capillary by blowing Ar gas into the crucible (pressure 3 bars). Once the capillary tube was infiltrated by the alloy, the crucible was lowered at 2 mm/min until it was immersed 20 mm into the liquid metal cooling bath. The whole system was equilibrated for 2 h and directional solidification was then performed for 1 h at a velocity $v_p < v_c$. At the end of solidification, a fast quench into the liquid metal bath ensured that the interface motion during quenching was negligible compared to the thickness of the solute boundary layer. Under such conditions, the liquid ahead of the planar interface solidified with a very fine microstructure. Composition profiles in the solid and quenched liquid were measured by an electron probe microanalyzer (EPMA). The composition measurements were averaged on a 500 μm line scan parallel to the quenched planar interface. While 10 points were measured in the solid on a line scan for each distance from the interface, the values of 30 point measurements were averaged in the quenched liquid. The standard deviation of Cr compositions for a line scan in the solid and quenched liquid was about 0.005 wt% Cr. (On a side note, the distance from the interface was not corrected with respect to the contraction of the alloy during the quench).

Using the constitutional undercooling criterion (Eq. 4) and the estimated data: $D_\ell = 2 \times 10^{-9}$ m²/s, $\Delta T_0 = 1$ K and $G = 100$ K/cm, a critical velocity v_c for Al–0.08 wt%Cr was predicted to be 20 μm/s. However, a lower (and safer) pulling speed of 5 μm/s was used, thus also giving an extended solute boundary layer and accordingly a better resolution of the Cr profile in the quenched liquid.

4. Results and discussion

Fig. 3(a) shows the EPMA results for the Cr distribution in an Al–0.08 wt%Cr sample. The quenched liquid ahead of the steady-state front has a lower composition, thus indicating that $k > 1$ in Al–Cr, i.e., the slope of the liquidus m_ℓ is positive. Please note that the solid–liquid interface position could only be determined by the abrupt drop of the Cr profile due to the low Cr content and, therefore, insufficient phase contrast in optical microscopy and SEM investigations. Chromium being depleted in the liquid ahead of the solid–liquid interface, this clearly shows that the invariant temperature is above the melting point of Al, i.e., the invariant is a peritectic. This method has the advantage that it does not depend on the delicate measurement of small temperature differences and gives an unambiguous demonstration of a peritectic reaction

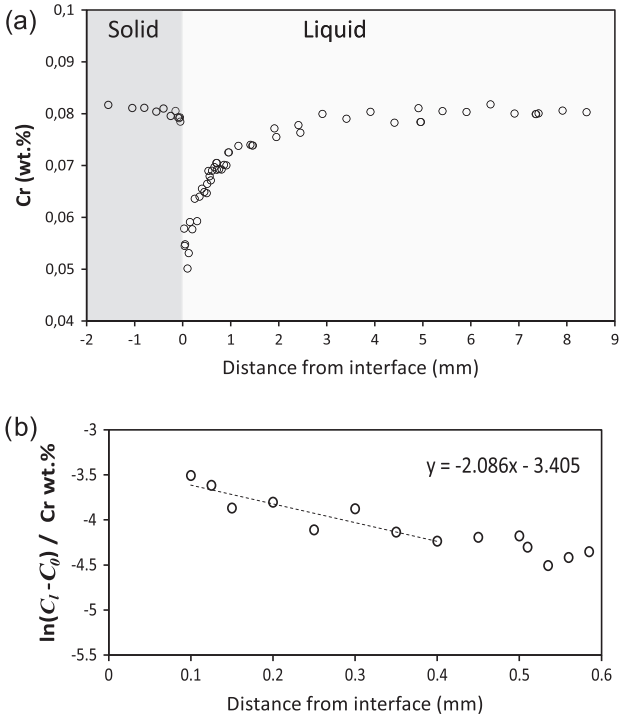

Fig. 3. (a) Cr distribution near the planar solid–liquid interface of Al–0.08 wt%Cr solidified at $v_p = 5$ μm/s and $G = 100$ K/cm during steady state solidification after 3600 s. (b) Logarithmic plot of the solute distribution, $\ln(C_\ell - C_0)$, in the quenched liquid with the distance from the interface for Al–0.08 wt%Cr.

between liquid, fcc-Al and $Al_{45}Cr_7$. Shibata et al. [26] had also observed Cr depletion in the liquid ahead of the solid–liquid interface in planar growth solidification experiments of Al–0.2 wt%Cr alloys. This result is in contradiction with the two recent studies in the literature showing a eutectic reaction on the Al-rich side of the Al–Cr system [13,15]. While the onset temperature of fcc-Al melting can be significantly affected by the impurity levels, impurities do not have such a dramatic effect on the nature of the reaction type. The interaction between the various solute elements for such a low concentration (about 100 ppm impurity in our alloys) is negligible.

The solid composition at the interface and liquid composition far from the interface are equal to the nominal composition of the alloy, indicating that steady state had been reached after 3600 s of solidification at constant pulling speed. Thus, Eq. (1) can be used to represent the liquid composition profile, and the plot of $\ln(C_\ell/z) - C_0)$ vs. distance from the interface, z, gives a straight line with a slope equal to $-v_p/D_\ell$, as shown in Fig. 3(b). Therefore, the diffusion coefficient of Cr in the liquid was deduced by a least squares method using these solute measurements up to 0.4 mm distance, where the errors are relatively small. A value $D_\ell = 2.4 \times 10^{-9}$ m²/s, was obtained, in close agreement with the measurement of Shibata et al. [26], i.e., 2.28×10^{-9} m²/s. The solute

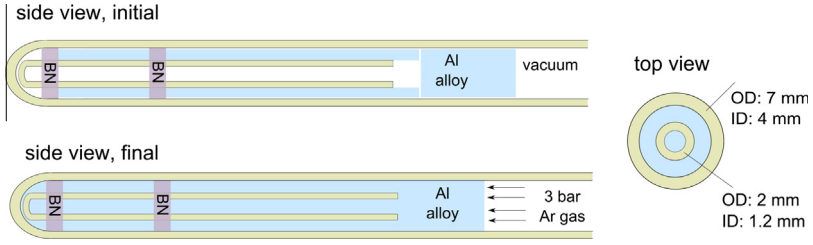

Fig. 2. Sample set up for planar growth experiments.

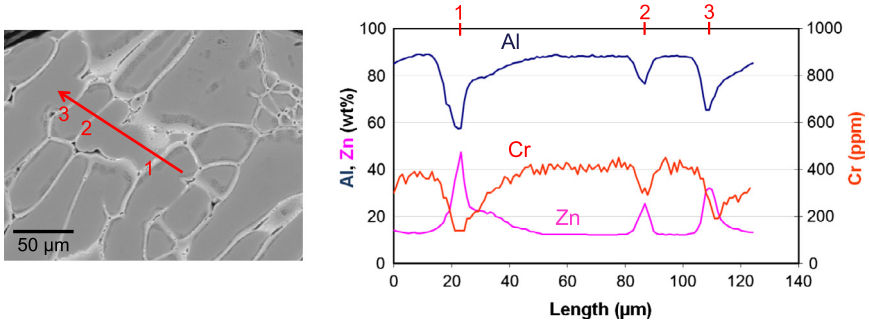

Fig. 4. EPMA of Al–20 wt%Zn–0.02 wt%Cr alloy solidified in a Bridgman furnace at $v_p = 4$ mm/min (67 μm/s) and $G = 50$ K/cm. A line scan was done along the red line and in the arrow direction shown in the micrograph. The interdendritic regions 1–3 are mentioned on both micrograph and composition profiles. (For interpretation of the references to colour in this figure legend, the reader is referred to the web version of this article.)

composition in the liquid at the solid–liquid interface, C_ℓ^*, was obtained by extrapolating this linear fit back to the interface position and ignoring the measured values close to the interface. This gave the value of the partition coefficient $k = 1.71$, in good agreement with the phase diagram of Murray ($k = 1.75$) [4].

As a final remark, the peritectic nature of the invariant at low Cr-content in the Al–Cr system was confirmed by the solidification of Al–Zn–Cr alloys [27,28]. Under much faster solidification conditions which produced dendrites, an Al–20 wt%Zn–0.02 wt%Cr alloy was solidified in a standard Bridgman furnace at $v_p = 4$ mm/min and with $G = 50$ K/cm. After quenching to limit back-diffusion in the solid, the composition profile across two dendrite arms was measured. Fig. 4(b) shows such an EPMA composition profile. As can be seen, while the composition profiles for Al and Cr have a similar behavior, that of Zn has a reverse trend. The core of the dendrites is richer in Al and Cr as compared with the quenched interdendritic liquid (positions 1, 2, 3 indicated in Fig. 4). This shows that the partition coefficient of Zn in this alloy is smaller than 1, as expected from the well-known eutectic-type binary phase diagram of Al–Zn, while that of Cr is greater than 1, thus confirming the peritectic nature of this element in Al–Zn–Cr alloys.

5. Conclusion

As a conclusion, in the planar front solidification experiments of Al–Cr alloys, Cr depletion in the liquid ahead of the quenched interface proves unambiguously the peritectic reaction on the Al-rich side of the Al–Cr system. This contradicts the recent studies in which the nature of the reaction was identified by thermal analysis of Al–Cr alloys or deduced from the solidification morphologies. The diffusion coefficient of Cr in liquid Al, as well as its partition coefficient, have also been deduced from the solute distribution profile in the liquid and solute jump at the quenched planar interface.

Acknowledgement

The authors wish to thank Constellium CRV, France for its financial support and Dr. Philippe Jarry for fruitful discussions.

References

[1] M. Audier, M. Durand-Charre, E. Laclau, H. Klein, J. Alloys Comp. 220 (1995) 225.
[2] B. Grushko, B. Przepiórzyński, D. Pavlyuchkov, J. Alloys Comp. 454 (2008) 214.
[3] K. Mahdouk, J.-C. Gachon, J. Phase Equilibria 21 (2000) 157.
[4] J.L. Murray, J. Phase Equilibria 19 (1998) 367.
[5] A.R. Harding, G.V. Raynor, J. Inst. Met. 80 (1952) 435.
[6] M.J. Cooper, Acta Crystallogr. 13 (1960) 257.
[7] Z.B. He, B.S. Zou, K.H. Kuo, J. Alloys Comp. 417 (2006) L4.
[8] W.L. Fink, H.R. Freche, Trans. AIMME, Inst. Met. Div. 104 (1933) 325.
[9] A.J. Bradley, S.S. Lu, X. An, J. Inst. Met 60 (1937) 319.
[10] H. Zoller, Schweizer Arch. Angew. Wiss. Und Tech. 26 (1960) 478.
[11] M. Goto, G. Dogane, Nihon Kogyokwaishi (1927) 931.
[12] J.G. Costa Neto, S. Gama, C.A. Ribeiro, J. Alloys Comp. 182 (1992) 271.
[13] Y. Du, J.C. Schuster, Y.A. Chang, J. Mater. Sci. 40 (2005) 1023.
[14] H. Okamoto, J. Phase Equilibria Diffus. 29 (2008) 112.
[15] A. Almeida, R. Vilar, Scr. Mater. 63 (2010) 811.
[16] T.B. Massalski, J.L. Murray, L.H. Bennett, H. Baker, Binary Alloy Phase Diagrams, American Society for Metals, Metals Park, OH, 1986.
[17] U.R. Kattner, B.P. Burton, Phase Diagrams Bin. Iron Alloy. (1993) 12.
[18] W.J. Boettinger, U. Kattner, K.Moon, J. Perepezko, DTA and heat-flux DSC measurements of alloy melting and freezing. Citeseer, 2006.
[19] ASTM Standard E928-08, Standard Test Method for Determining Purity by DSC, ASTM International, West Conshohocken, PA, 2008. doi:10.1520/E0928-08, <http://www.astm.org>.
[20] S. Dobler, T.S. Lo, M. Plapp, A. Karma, W. Kurz, Acta Mater. 52 (2004) 2795.
[21] J.H. Lee, J.D. Verhoeven, J. Cryst. Growth 144 (1994) 353.
[22] F. Kohler, L. Germond, J.-D. Wagnière, M. Rappaz, Acta Mater. 57 (2009) 56.
[23] J. Valloton, J.-D. Wagnière, M. Rappaz, Acta Mater. 60 (2012) 3840.
[24] Y. Liu, F. Lan, G. Yang, Y. Zohou, J. Cryst. Growth 271 (2004) 313.
[25] W.A. Tiller, K.A. Jackson, J.W. Rutter, B. Chalmers, Acta Metall. 1 (1953) 428.
[26] K. Shibata, T. Sato, G. Ohira, J. Cryst. Growth 44 (1978) 435.
[27] G. Kurtuldu, Influence of Trace Elements on the Nucleation and Solidification Morphologies of Fcc Alloys and Relationship with Icosahedral Quasicrystal Formation, No 6057, École Polytechnique Fédérale de Lausanne, 2014.
[28] G. Kurtuldu, P. Jarry, M. Rappaz, Acta Mater. 61 (2013) 7098.